remote sensing

Article

Runoff Responses of Various Driving Factors in a Typical Basin in Beijing-Tianjin-Hebei Area

Zhaohui Feng [1,2,†], Siyang Liu [1,3,†], Yikai Guo [4] and Xiaojie Liu [1,*]

[1] Key Laboratory of Natural Resource Coupling Process and Effects, Ministry of Natural Resources, Institute of Geographic Sciences and Natural Resources Research, Chinese Academy of Sciences, Beijing 100101, China
[2] University of Chinese Academy of Sciences, Beijing 100049, China
[3] Chinese Academy of Environmental Planning, Beijing 100041, China
[4] Ecological Environment Planning and Environmental Protection Technology Center of Qinghai Province, Xining 810007, China
* Correspondence: liuxj@igsnrr.ac.cn
† These authors contributed equally to this work and should be considered co-first authors.

Abstract: Changes in land use and landscape caused by human activities, rapid socioeconomic development and climate change disturb the water cycle process and impact the runoff. This study analyzed the runoff responses to different driving factors in a typical basin in the Beijing-Tianjin-Hebei region of North China combined with methods such as geographically and temporally weighted regression, landscape pattern indexes and Budyko theory. The results indicated that the runoff and runoff depth were higher in the central and south part and were lower in the northwest of the basin. Furthermore, the average runoff increased at the later stage of the study period. Artificial surface and land use intensity exerted positive impacts on runoff and runoff depth in most areas. The complex and diverse landscape with a high shape index blocked runoff to some extent. Moreover, runoff depth would increase by 0.724 mm or decrease by 0.069 mm when the rainfall or potential evaporation increased by 1 mm. In addition, population density and the economic development in both rural as well as urban areas put a heavy burden on runoff and water resource in this basin. From above it could be concluded that the impacts on runoff due to environmental change brought by human activities could not be neglected though the runoff was also greatly affected by climate change. This study reflected the runoff responses to driving factors in a typical basin of North China, which will provide reference for water resource protection and give enlightenment to water management.

Keywords: runoff response; land use change; landscape pattern evolution; climate change; socioeconomic development

check for updates

Citation: Feng, Z.; Liu, S.; Guo, Y.; Liu, X. Runoff Responses of Various Driving Factors in a Typical Basin in Beijing-Tianjin-Hebei Area. *Remote Sens.* **2023**, *15*, 1027. https://doi.org/10.3390/rs15041027

Academic Editor: Giovanni Battista Chirico

Received: 5 January 2023
Revised: 23 January 2023
Accepted: 6 February 2023
Published: 13 February 2023

1. Introduction

In the earth system, the hydrological cycle is regarded as the significant substance as well as the energy cycle, and runoff generation has always been an essential issue in the hydrology process in the changing environment in the past 20 years [1]. Analyzing the runoff change trends has been a challenge in water resource management because it is a significant indicator in measuring if the water resource is able to be supplied constantly [2]. There was runoff variation due to the changed hydrological process caused by human activities and climatic factors [3]. In addition, many external factors impacted the water balance and even caused land subsidence [4]. For example, the Beijing-Tianjin-Hebei urban agglomeration formed the biggest groundwater funnel in the world [5]. Thus, it is necessary to grasp the runoff change laws and the behind driving factors so as to form efficient policies on managing water resources for decision makers [6].

Runoff variations are affected by many factors, including both natural and human aspects such as land use change, landscape pattern evolution, climate change and socioeconomic development. Previous study pointed out that land use change could change the proportion of surface runoff, groundwater recharge, interflow etc., and the available water in this area could be affected accordingly [7]. The human activities that led to land use change such as deforestation, agricultural expansion, grazing expansion, wood burning and urbanization will change the hydrological processes including runoff, base flow, infiltration and so on [8]. Landscape pattern evolution also affects the hydrological and ecological processes of the terrestrial ecosystem such as the biogeochemical cycle and the water cycle. It changes the processes of runoff generation and runoff confluence and impacts the cycles of water resource and hydrology when the land surface is the underlying surface [9]. When the landscape pattern was changed by water conservancy projects and farmland reclamation, the formation, transformation as well as distribution of runoff would be altered. Then a series of subsequent extreme hydrological events caused soil erosion [10]. As reported, climate change not only altered the water cycle process and runoff, but also affected the regional water balance through changing the evaporation and precipitation of the region. In addition, the runoff in some regions decreased obviously due to the increasing evaporation and the reduced rainfall [11]. Thus, it has become one of the hotpots to explore climatic impact on the hydrological cycle and many studies about the climatic effects on the runoff have already been conducted at the watershed, regional or global in scale [12,13]. In addition, the groundwater overexploitation caused land subsidence and imposed a heavy burden on the water cycle under the socioeconomic development in some urban agglomerations such as those in the Beijing-Tianjin-Hebei region [14]. While adequate water supply is indispensable to social and economic development and citizen life. Considering the above factors, it is important to conduct research on the relationships between the changes of land use, landscape pattern, climate as well as social economy and runoff.

In current studies, water balance theory based on the Budyko hypothesis as well as model-simulation approaches are both important methods for exploring the reasons for runoff variation. The water balance method not only has valid physical meaning compared with traditional empirical approaches, but also has a simple process and easily accessible parameters, which cause it to be popular and widely used [15]. A double mass curve is widely used in studying the hydro-climatic consistency, which is a practical and simple method [12,16]. In addition, it is usually adopted to detect the contribution from driving factors to runoff [16]. Furthermore, geographically and temporally weighted regression (GTWR) considers both spatiotemporal heterogeneity and autocorrelation of the variables, which explains the temporal and spatial relationships between the dependent variables and their explanatory variables better [17]. In addition, it performed better than many mathematical statistical methods such as the ordinary least squares model and geographically weighted regression as proved [18]. Furthermore, gray correlation analysis (GCA) is used to calculate the correlation degree between variables from various systems, which can quantify the relationship between driving factors and hydrological elements [19].

The Beijing-Tianjin-Hebei region in China has intensive human activity, which contributed a lot to the reshaping of land use as well as landscape pattern and is prone to have impact on the runoff [20]. In addition, the high population density, rapid urbanization and socioeconomic development here exploited about 20 billion cubic meters of groundwater each year, which formed the hugest groundwater funnel under the urban agglomeration in this region [14]. Moreover, the runoff here was impacted by climatic conditions because rainfall was brought by monsoons in temperate monsoon region. The fluctuated runoff would change groundwater depth and affect industrial, residential and agricultural water usage [3]. Therefore, this research aims to (1) explore the spatial and temporal evolution trends of runoff and runoff depth; (2) uncover the responses of runoff and runoff depth to land use changes and landscape pattern evolutions; and (3) analyze the influences on runoff and runoff depth from climatic factors as well as the correlation degrees between runoff, runoff depth and socioeconomic indicators. This research focuses on the responses to runoff and runoff depth of various driving factors which will give enlightenment to the protection and efficient utilization of water resources in densely populated and highly developed areas.

2. Material and Methods

2.1. Study Area

The typical basin with the area of about 3.95×10^4 km^2 for this research is located in the north region of the Beijing-Tianjin-Hebei region in China (Figure 1). The annual runoff and runoff depth were measured in each monitoring site and the basin was divided into many sub-basins (the sub-basin division in this study is from https://www.hydrosheds.org/hydroatlas, accessed on 15 June 2022). The northwest region of the typical area has the higher terrain and the southeast region has the lower terrain, which cause the altitude to change between 128 and 2232 m. This basin has chestnut soil, cinnamon soil, etc. The alluvial parent soil is distributed along the banks of large rivers, with flat terrain and good natural conditions. In addition, the parent material of diluvium with less mineral composition and poor nutrition does not have uniform soil texture. Moreover, the loess parent material is widely distributed in this basin. The soil is deep and moderate in texture, rich in nutrients and has strong water retention and drought resistance. A calcic layer and sandy gravel layer and so on are the soil barrier layers of this basin [21].

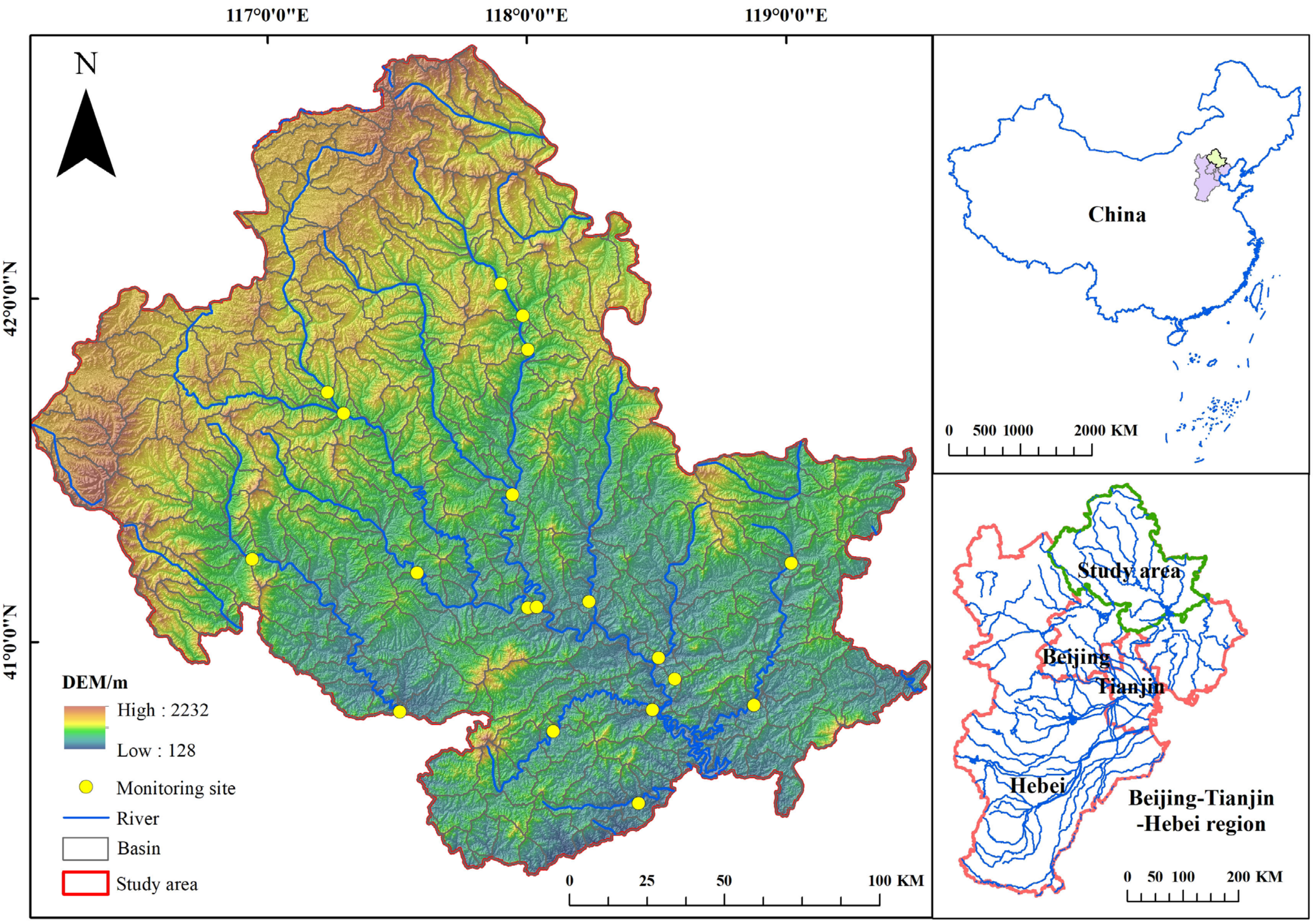

Figure 1. Study area.

The study region has a temperate monsoon climate [20]. The monsoon brings precipitation to the region from the sea in summer, which makes it a climate characterized by high temperature and rainfall in summer as well as dry and cold in winter. The annual precipitation is 400~800 mm in this basin. The Panjiakou dam in the downstream of this basin plays a role in adjusting runoff [22]. Moreover, this basin provides a water resource for its downstream cities such as Beijing and Tianjin, which are the megacities with a population of over 10 million [23]. Beijing-Tianjin-Hebei region with increased population, changed land use as well as landscape and rapid economic development, is supposed to choose this typical basin to give more attention to runoff change [24,25].

2.2. Runoff, Runoff Depth and Potential Evaporation

The runoff (10^8 m^3) and runoff depth (mm) for each monitoring site (2006–2018) were obtained from the Institute of Geographical Sciences and Natural Resources Research of Chinese Academy of Sciences (http://www.igsnrr.ac.cn/, accessed on 28 June 2022). The potential evaporation (*PET*, mm) data and other climate data used in this study were acquired from http://www.geodata.cn/ (accessed on 15 July 2022), which was calculated by Hargreaves theory [26].

$$PET = 0.0023 \times S_0 \times 0.5(MaxT - MinT) \times (MeanT + 17.8) \quad (1)$$

where *MeanT*, *MaxT* and *MinT* represent the monthly average, maximum and minimum temperature (°C), respectively. S_0 denotes the theoretical solar radiation reaching the top of the Earth's atmosphere. The annual *PET* in the study is the sum of the monthly *PET*.

2.3. Climate Impact Based on Budyko Theory

Since the average evaporation in the long time series of the basin depends on the potential evaporation or net radiation and the water supply from the atmosphere, the evaporation can be expressed as a function of potential evaporation and precipitation, as shown in Formula (2):

$$\frac{ET}{P} = f(PET/P) \quad (2)$$

where P is rainfall (mm), *PET* and *ET* refer to potential evaporation (mm) and actual evaporation (mm), respectively. The differential form of Budyko theory is derived in combination with the physical meaning of hydrometeorology, thus forming the analytical formula of the theory [27]:

$$\frac{ET}{P} = 1 + \frac{PET}{P} - \left[\left(\frac{PET}{P}\right)^{\omega} + 1\right]^{1/\omega} \quad (3)$$

The runoff depth simulation formula can be derived according to the water balance formula $P = ET$ + runoff depth in long time series:

$$\text{runoff depth} = [P + PET^{\omega}]^{1/\omega} - PET \quad (4)$$

In addition, the runoff depth sensitivities to rainfall and *PET* are obtained by combining differential partial derivative:

$$\frac{\partial \text{runoff depth}}{\partial P} = \left[1 + \left(\frac{PET}{P}\right)^{\omega}\right]^{(1/\omega - 1)} \quad (5)$$

$$\frac{\partial \text{runoff depth}}{\partial PET} = \left[1 + \left(\frac{P}{PET}\right)^{\omega}\right]^{(1/\omega - 1)} - 1 \quad (6)$$

ω in Formulas (5) and (6) needs to be solved by the least squares. Then, the runoff depth changes caused by climate change can be quantified as follows [28,29]:

$$\Delta \text{runoff depth} = \beta \Delta P + \gamma \Delta PET \quad (7)$$

Furthermore, the sensitivity coefficients β, γ are the influence amount of unit P and unit *PET* on runoff depth.

2.4. Geographically and Temporally Weighted Regression

The geographical regression relationship between land use and runoff could be explored by GTWR because the correlations between explanatory variables and dependent variable could be calculated considering both temporal and geographical factors [18]. In order to explain the nonstationary during parameter calculation, weight matrix is constructed using the distances between the dependent variable and its explanatory variables determined by spatiotemporal coordinates (x, y, t) [30].

GTWR formula is as:

$$Y_i = \lambda_0(x_i, y_i, t_i) + \sum_j \lambda_j(x_i, y_i, t_i) X_{ij} + \varepsilon_i \tag{8}$$

where Y_i and X_{ij} denote the dependent variable in the ith location and its jth explanatory variable, respectively. In addition, the regression coefficient γ_j (x_i, y_i, t_i) of the jth explanatory variable in location i can be calculated as:

$$\hat{\gamma}(x_i, y_i, t_i) = \left[X^T(\mathrm{diag}(\alpha_{i1}, \alpha_{i2}, \ldots, \alpha_{in}))X\right]^{-1} X^T(\mathrm{diag}(\alpha_{i1}, \alpha_{i2}, \ldots, \alpha_{in}))Y \tag{9}$$

where α_{ij} ($1 \leq j \leq n$) corresponding to the weights under the calibrated weighted regression of the ith observation, which is the representation of space–time distance functions of (x, y, t). In GTWR, the observations closer to location i are assumed to have greater impact than farther observations when estimating γ_j (x_i, y_i, t_i).

Moreover, the optimum kernel bandwidth can be chosen using the corrected Akaike information criterion [31]:

$$AIC_c = n\ln(2\pi) + 2n\ln(\hat{\sigma}) + n\left\{\frac{n + \mathrm{tr}(A)}{n - 2 - \mathrm{tr}(A)}\right\} \tag{10}$$

where tr(A) is the trace of projection matrix, which is between prediction $\widehat{Y}$ and its observation γ. In addition, $\widehat{\sigma}$ is the prediction variance of random error. Bandwidth with the minimum AIC_c can be selected as the best bandwidth. The land use data for GTWR calculation was developed by [32].

2.5. Gray Correlation Analysis

The gray correlation degree is used to measure the correlations of the variables from socioeconomic system and runoff. Its core idea is to judge the closeness of their relationships by using the geometric similarity of the reference variable (runoff or runoff depth) and the comparison variable (socioeconomic indicators) [33]. If two variables have the consistent change trend, there is high correlation degree between them. Otherwise, the correlation degree is low. The main steps of gray correlation analysis are as follows [34]: First, determine the reference sequence X_0 and its comparison sequences [X_1, X_2, ... , X_n] and use the following formula to make them have the unified dimension.

$$X(k) = X(k)/X_{mean} \tag{11}$$

where $X(k)$ and X_{mean} are the elements of comparison sequence and the average of this comparison sequence, respectively.

Then, the correlation coefficient is calculated as:

$$\beta(X_0(e), X_i(e)) = \frac{\min_{ie}|X_0(e) - X_i(e)| + \rho\max_{ie}|X_0(e) - X_i(e)|}{|X_0(e) - X_i(e)| + \rho\max_{ie}|X_0(e) - X_i(e)|} \tag{12}$$

where $X_0(e)$ and $X_i(e)$ are the eth element in reference sequence X_0 and comparison sequences X_i, respectively.

$$Cor_i = \frac{1}{N}\sum_{e=1}^{N}\beta(X_0(e), X_i(e)) \quad (13)$$

where Cor_i and N are the correlation degree between $X_0(e)$ and $X_i(e)$ and the sequence length. The five annual socioeconomic indicators for gray correlation analysis were extracted from Chengde statistical yearbook [35], which were per capita gross domestic product (CNY), population density (person/km^2), industrial output density (CNY/km^2), per capita disposable income of rural residents (CNY) and per capita disposable income of urban residents (CNY).

2.6. Landscape Pattern Indexes

Eleven landscape pattern indexes were selected, including patch density (PD), number of patches (NP), largest patch index (LPI), edge density (ED), mean shape index (SHAPE_MN), landscape shape index (LSI), mean Euclidean nearest neighbor (ENN_MN), patch cohesion index (COHESION), contagion index (CONTAG), aggregation index (AI) and Shannon's diversity index (SHDI). Specifically, NP denotes the number of patches in the basin and PD represented the density of certain patches in the watershed landscape. LPI is the proportion of the largest patch in a certain patch type to the whole landscape area, which reflects the dominant species in the landscape and reflects the direction and intensity of human activities. ED is the length of landscape element boundary per unit area [36].

Moreover, SHAPE_MN describes the patch structure of the landscape as that of the average patch characteristic, which provides a measure of central tendency in the corresponding patch characteristic. LSI reflects the shape complexity of the overall landscape and ENN_MN is used to measure the Euclidean Nearest Neighbor Distance Distribution. COHESION is able to reflect the combination degree between patches in the landscape, and CONTAG represents the agglomeration degree or extension trend of different patch types in the landscape. AI is usually adopted to describe the aggregation of the landscape. SHDI based on information theory is a measurement index to measure the diversity of ecological landscape [36]. The chosen indexes were able to represent the landscape patch characteristics, landscape shape, landscape aggregation degree well. FRAGSTATS software was used to calculate the above indexes on the landscape scale [37].

3. Results and Discussion

3.1. Interannual Variation of the Runoff and Runoff Depth

The change of the average runoff and depth of runoff monitoring stations (Figure 1) over time in the typical basin is shown in Figure 2. It is shown that the regional runoff increased at the later stage of the study period. In addition, 2008, 2011, 2012 and 2018 were the years with higher runoff compared with adjacent years, while 2009 and 2014 were located at the "valley" of the runoff curve, reflecting the overall reduction of runoff in these years (Figure 2a).

Figure 2b shows that the runoff depth in the basin also increased in 2018 compared to that of 2006, and the slope of its trend line was larger than that of the runoff [38]. In addition, although the annual average of 2008, 2011 and 2012 were located at the "peak" of the runoff depth curve, the runoff depth in 2008 was significantly lower than that in 2011 and 2012. However, the runoff depth in 2018 was extremely higher than that in 2011 and 2012, which was also different from the runoff curve in the corresponding years. In addition, 2009 and 2014 were located at the "valley" of the runoff depth curve, which was similar with the runoff curve. In addition, the runoff depth and runoff were low in 2006, which implied that the surface water resources were not abundant in these years. This phenomenon may be due to the reduction in natural water sources such as rainfall, or may be related to other anthropic factors [39].

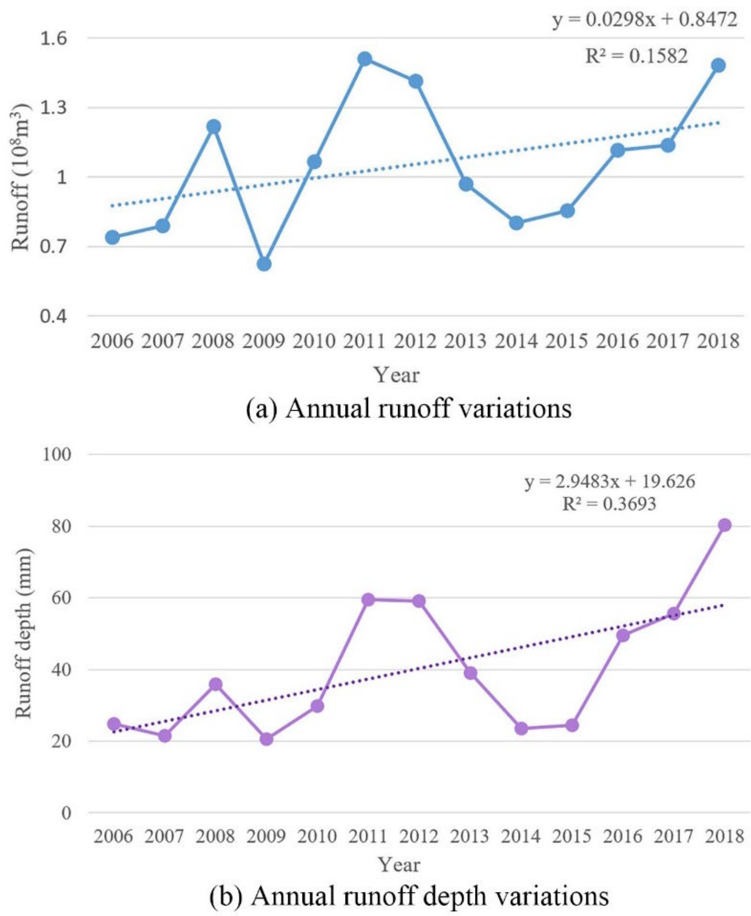

Figure 2. Annual variations of runoff and runoff depth.

3.2. Spatial Distribution of Runoff and Runoff Depth

The spatial distribution of runoff in the hydrological monitoring sites (Figure 3) displayed that the sites with the most abundant runoff were in the central and south central area of the study region and they had always been rich in water resources during the study period. In addition, most of the monitoring points showed an increasing trend of runoff in subsequent years (2016–2018) although the runoff in the south area was not very rich (Figure 3a). Except for the natural factors such as rainfall and evaporation, the cause for this phenomenon may be related to human activities in subsequent years, such as inter-basin water transfer, reservoir construction, agricultural irrigation, water drainage and supply in urban and other water conservancy projects and measures [40–42]. Different from the above situation, Figure 3a showed that the runoff of most monitoring points in the northern part of the basin was low throughout the study period, reflecting the unequal distribution of the water resources in this area. The basin with high terrain in the northwest and low terrain in the southeast was also prone to collecting more tributaries and water resources in the south area regardless of the climatic factors and human activities, which had become an important reason for the uneven distribution of water resources [43].

Figure 3b shows that the monitoring points in the southern part of the basin usually had large runoff depth, especially at some points in 2016, 2017 and 2018. In addition, the runoff depth at the northern points of the basin was low as well. However, unlike the runoff, there was no monitoring point with large runoff depth in the middle of the basin, which may be related to the drainage area of this region [44].

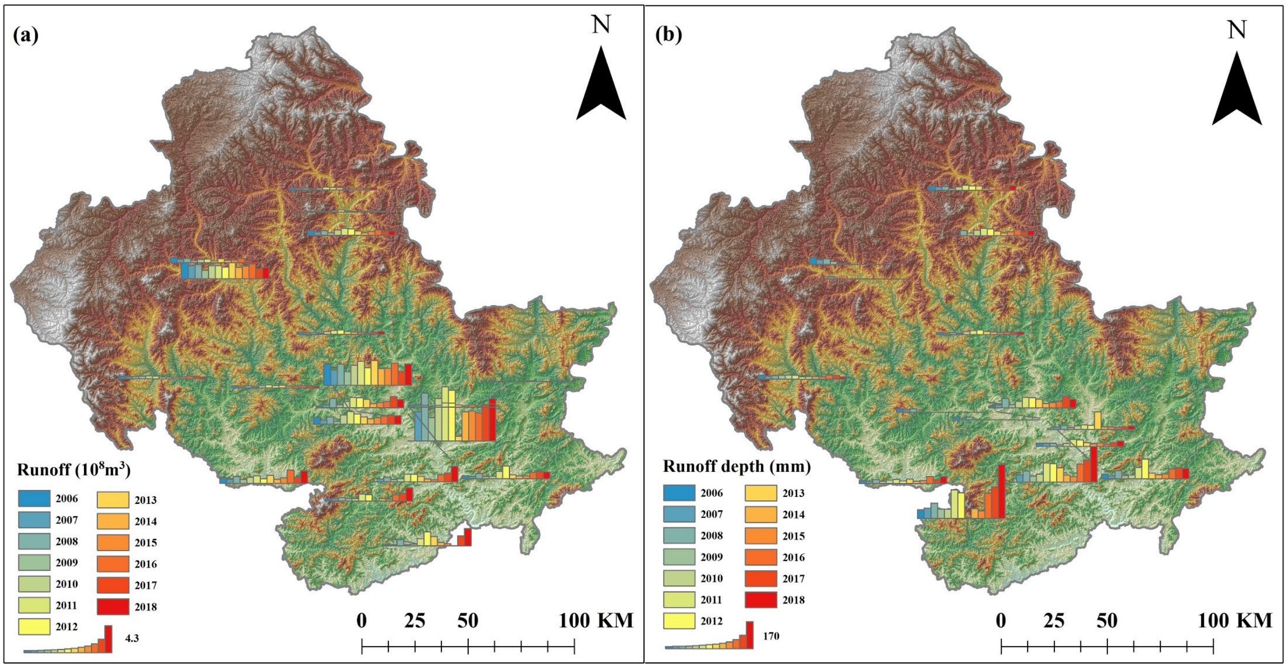

Figure 3. Annual spatial distribution of runoff and runoff depth. (**a**,**b**) were the spatial distribution for annual runoff and annual runoff depth, respectively.

3.3. Response of Runoff and Runoff Depth under Land Use Change

Cropland was converted into 194.50 km^2 of forest and 379.33 km^2 of grassland, and grassland was converted to 203.41 km^2 of cropland and 503.46 km^2 of forest from 2006 to 2010 (Table 1). The large amount of cropland and grassland transferred into other land uses and other land uses transferred into forest caused the average runoff of the watershed to increase from 0.83×10^8 m^3 in 2006 to 1.07×10^8 m^3 in 2010 (Figure 2a). Some studies had pointed out that the increase in forest would increase evaporation and reduce watershed runoff. While agricultural machinery or livestock in agricultural activities would compact the soil, reduce soil pores and soil permeability, so as to reduce the amount of water absorbed by the soil and increase surface runoff, thus the runoff reduction from 2006 to 2010 may be caused by the increase in cropland though the increasing forest adjusted runoff to some degree [45].

With the time evolution, 132.75 km^2, 351.84 km^2 and 60.24 km^2 of cropland were converted into forest, grassland and artificial surface from 2010 to 2014, respectively (Table 1). In addition, grassland was converted into 241.04 km^2 of cropland and 678.09 km^2 of forest. It is reported that the conversion of cropland to artificial surface hardened the soil, reduced the infiltrated water and caused a considerable amount of water to flow into the river and increased the runoff [46]. However, the soil structure of the transferred forest and grassland would improve the soil permeability, reduce the surface runoff, and the runoff depth would also be reduced. Furthermore, previous studies had pointed out that the water absorption ofroots in forest soil was greater than that of grassland soil, so the large areas of the transferred forest in 2014 (680.04 km^2) further reduced surface runoff in 2014 (Figure 2a) compared with that in 2010 [47].

During 2014–2018, the conversion of 586.16 km^2 of grassland to cropland and 100.10 km^2 of cropland to impervious surface increased the average runoff from 0.80×10^8 m^3 in 2014 to 1.48×10^8 m^3 in 2018, and runoff depth from 22.26 mm to 68.39 mm (Figure 2a,b). The compacted soil contributed greatly to this result [45]. In contrast, 233.04 km^2 of cropland and 1535.05 km^2 of grassland were converted to forest, and 337.14 km^2 and 707.75 km^2 of forest were transferred to cropland and grassland, respectively (Table 1). Thus, the runoff may be also affected by the expanded forest area.

Table 1. Land use conversion matrix during 2006–2018 (km^2).

Period	Land Use	Forest	Grassland	Cropland	Water	Artificial Surface	Barren	Total
2006–2010	Forest	22,127.48	4.72	34.20	0	14.11	0	22,180.50
	Grassland	503.46	9932.74	203.41	1.03	13.06	0.19	10,653.88
	Cropland	194.50	379.33	5674.73	3.65	53.33	0	6305.54
	Water	0.71	0.58	2.40	38.28	0.58	0.01	42.55
	Artificial surface	0	0	0.02	1.99	364.53	0	366.54
	Barren	0	0.16	0.01	0	0.02	0.22	0.41
	Total	22,826.14	10,317.53	5914.77	44.96	445.62	0.42	3.95×10^4
2010–2014	Forest	22,695.19	4.29	103.24	0	23.42	0	22,826.14
	Grassland	678.09	9381.43	241.04	1.21	15.58	0.17	10,317.53
	Cropland	132.75	351.84	5364.74	5.20	60.24	0	5914.77
	Water	0.15	0.61	2.04	41.36	0.80	0.01	44.96
	Artificial surface	0	0	0.01	1.10	444.51	0	445.62
	Barren	0	0.11	0.03	0	0.03	0.26	0.42
	Total	23,506.18	9738.29	5711.09	48.86	544.57	0.44	3.95×10^4
2014–2018	Forest	22,425.79	707.75	337.14	1.47	28.74	0.06	23,506.18
	Grassland	1535.05	7584.94	586.16	1.47	27.07	0.66	9738.29
	Cropland	233.04	316.19	5056.18	4.67	100.10	0.03	5711.09
	Water	1.36	0.88	3.17	42.27	1.14	0.03	48.86
	Artificial surface	9.87	9.70	49.20	1.39	474.32	0.03	544.57
	Barren	0.03	0.12	0.02	0	0.03	0.23	0.44
	Total	24,205.90	8620.01	6031.99	51.27	631.41	1.05	3.95×10^4

The spatiotemporal heterogeneity of the influence of land use on runoff was quantified by geographically and temporally weighted regression (Figures 4 and S1–S7); the land use variables in explanatory variables were the land use areas of the sub-basin where each monitoring point was located. The explanatory variables in this study passed the collinearity diagnosis of variance inflation factor (VIF < 10). In addition, the accuracy of GTWRs for runoff and runoff depth are in Table S1.

The results showed that bare land without vegetation cover had a negative impact on runoff and runoff depth in most areas from 2006 to 2018 and this phenomenon was more obvious in the southeast of the study area. This was because natural vegetation such as forests would increase runoff in some environments. By contrast, when vegetation was destroyed and there was low vegetation coverage, the runoff was relatively low as a previous study confirmed. Because the decline in the capacity of vegetation to conserve water led to the reduction in flow in the dry season and the redistribution of runoff [48]. In addition, this would also reduce the water and soil conservation capacity of the basin. The impact that cropland reduced runoff was smallest in the northern region, while this impact increased gradually in the central and southern part of the basin. Furthermore, there was always a negative relationship between cropland and runoff depth in the southeast area (Figures S4–S7), which indicated that planting activities reduced the runoff production to a certain extent [49]. Previous studies have pointed out that the forest canopy and its litter intercepted precipitation, and the relatively porous forest soil had high permeability and water conductivity, which could reduce runoff to some degree [50]. Thus, the forest of the basin showed a negative effect on the runoff in the central and northern parts in 2006, 2010 and 2014, and in the northern part in 2018. Moreover, it also had a negative impact on the runoff depth during 2006–2018. The positive impact of forest in the southeast of the basin on runoff may be because the canopy with complex structure and lush branches as well as leaves strongly captured the condensed water such as fog, thereby increasing horizontal precipitation [51]. The northern and central grasslands of the watershed had a negative impact on runoff during 2006–2018, because the soil pores of the grassland transported water to the ground and reduced runoff. However, the positive impact of grassland on runoff may be due to the restriction of water inflow by the fine topsoil in the southeast, or the restriction of the interaction between the matrix and macropores below the topsoil [47].

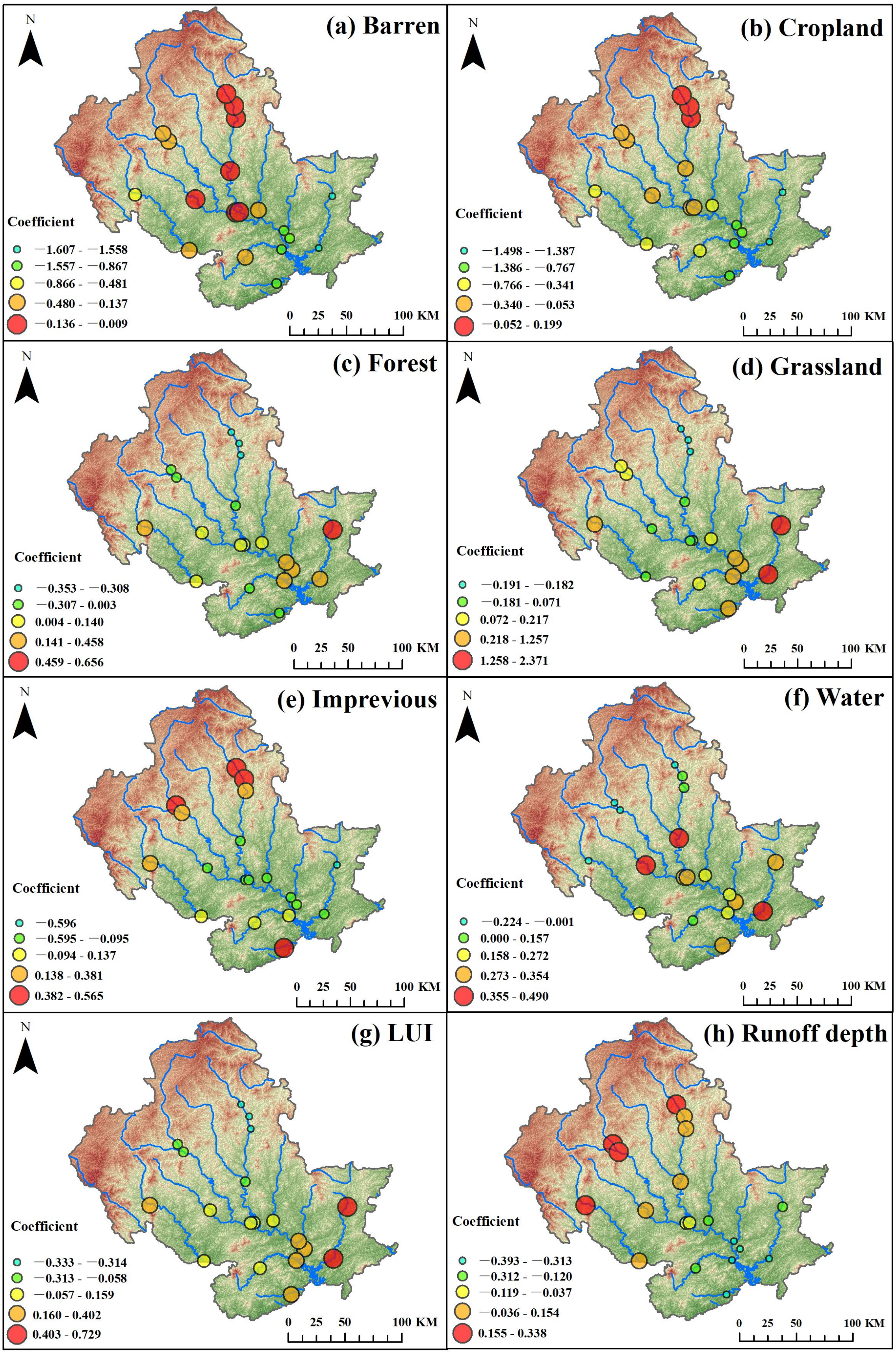

Figure 4. Geographically and temporally weighted regression between land use and runoff in 2018.

Some studies have proved that the constructed land had stronger runoff production capacity than forest and grassland [52]. The artificial surface in the north and south of the watershed was positively related to runoff in this study because the artificial surface significantly increased surface runoff in these areas. In addition, the results showed that the sub-basin with the larger water area had the larger of the runoff in the most monitoring positions. Furthermore, most of the runoff depth was also positively affected by the water area at the same time, which also confirmed the strong runoff production capacity of the water body [52]. During the study period, LUI had a positive impact on runoff except for the individual points in the north. In addition, it also had positive relationship with runoff depth except at some points in the middle. This was because the soil was compacted and the gap was reduced with the increase in human activities and land use intensity, resulting in the reduction of water infiltration into the soil and the increase of runoff [53]. The negative impact of some points may be due to their specific land use compositions in the sub-basins. In addition, the runoff and runoff depth were positively correlated in the northwest, but become negatively correlated in the southeast, which may be caused by the change in the watershed area.

3.4. Impacts on Runoff and Runoff Depth from Landscape Pattern

The annual landscape pattern indexes for the sub-basins where the monitoring points were located were calculated from 2006 to 2018, and the Pearson correlations between the landscape indexes and the runoff as well as runoff depth during this period were in Table 2 [54]. It can be discovered that patch density had a positive correlation with runoff, and it increased with time (Figure S8a). This reflected that the runoff process and the resulting soil erosion increased the patch density of the landscape, and this phenomenon became more and more obvious in the typical basin [55]. The mean shape index represented the complexity of landscape shape and the larger the SHAPE_MN the more complex the landscape shape of the basin. There were significant negative correlations between SHAPE_MN and runoff in the whole study period (Table 2) and in 2018 (Figure S8a), which was likely because the complex landscape diverted and blocked the runoff and brought about low runoff under the complex landscape [56,57].

Table 2. Pearson correlation coefficients between runoff and runoff depth as well as landscape indexes.

Landscape Pattern Index	Runoff	Runoff Depth
NP	0.113	−0.120
PD	0.247 *	−0.106
LPI	0.161	0.343 **
ED	−0.0938	−0.396 ***
LSI	−0.0878	−0.266 *
SHAPE_MN	−0.328 **	−0.233 *
ENN_MN	−0.0666	0.389 ***
CONTAG	0.179	0.367 **
COHESION	0.216	0.212
SHDI	−0.185	−0.344 **
AI	0.0983	0.401 ***

(***, $p < 0.001$; **, $p < 0.01$; *, $p < 0.05$).

LPI quantified the proportion of the landscape area composed of the largest patch in coverage. It was a simple dominance measure, which emphasized the significance of the largest patch [58]. In addition, it was positively related to the runoff depth in this study. Moreover, the shape of the patches in this basin were more irregular and complex when the edge density, LSI and SHAPE_MN became larger. When the runoff flowed along the contour of irregular patches, the runoff loss was larger, which caused the runoff depth to decrease [59]. SHDI illustrated the heterogeneity and complexity of the ecosystems. Generally speaking, the complexity of landscape structure increased with the increasing diversity index (Table 2), which enhanced the blocking effect of the landscape on the runoff and caused the negative correlation with SHDI and runoff depth [57,60]. Furthermore, this relationship became more obvious in the later research period (Figure S8a). When the CONTAG and AI became larger, the aggregation degree of the watershed landscape grew higher correspondingly, which had a positive effect on runoff depth (Table 2).

3.5. Influences on Runoff and Runoff Depth from Climate Factors

Previous studies had pointed out that rainfall had a significant impact on runoff, while drought changed their relationship and runoff coefficient [61,62]. The study in the Campaspe River Basin in southeast Australia showed that when rainfall reduced by 15% per year, the runoff reduced by 59% in this region [63]. In this study, the variation trends of rainfall, runoff and runoff depth in the study area were consistent in 2006–2010 and 2012–2017 (Figures 2a,b and 5). Rainfall had a significantly positive impact on runoff and runoff depth in most years of the study period. The different amounts of potential evaporation and precipitation control the distribution of precipitation to actual evaporation and runoff from the perspective of climatology [64]. Previous studies had shown that the potential evaporation changed with the changes in radiation and aerodynamic variables affected by the ground environment and climate change [65]. In this study, when the rainfall increased and the temperature decreased, the potential evaporation also decreased, which increased the runoff and runoff depth in the corresponding period (2007–2008, 2009–2010, 2014–2016, 2017–2018). This was because rainfall supplemented this region with more external water and the decreased evaporation as well as the temperature carried less water into air, which caused less water supply loss to runoff [66]. In contrast, the reduction in rainfall decreased the amount of regional water resources, and the rising temperature as well as the increasing evaporation, which all reduced the runoff in some periods (such as 2013–2014). This was because insufficient water supplementary to this region decreased runoff as a result.

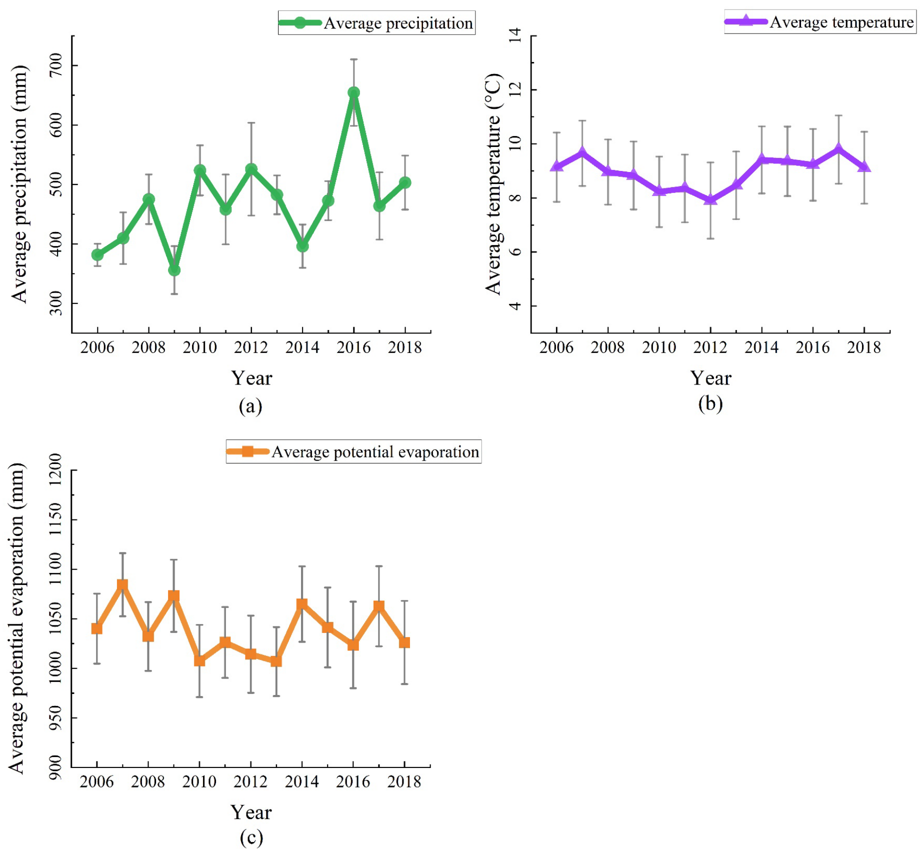

Figure 5. Annual change of climate factors. (**a**–**c**) were the annual average precipitation, temperature and potential evaporation, respectively.

Budyko theory had been applied as a balanced interpretation of river climate elasticity successfully [67]. The analytical framework developed based on the Budyko curve determined the runoff sensitivity to potential evaporation, precipitation and catchment characteristics well in Australia [68]. In this study, the parameter ω = 1.3121 in Budyko's hypothesis theory. The watershed runoff sensitivity coefficient to precipitation ranged from 0.674 to 0.783 and the multi-year average sensitivity coefficient was 0.724 (Figure 6a) according to Formulas (5) and (6). This indicated that the runoff of the basin was sensitive to rainfall. When the rainfall increased by 1mm, the runoff depth would increase by 0.724 mm during 2006–2018. However, the annual runoff sensitivity to rainfall fluctuated and its change trend was roughly consistent with precipitation in this basin (Figure 6a). In addition, the multi-year average runoff sensitivity coefficient to potential evaporation was −0.069 and the range of the sensitivity coefficient was −0.100 to −0.049. The result conveyed that the runoff depth decreased by an average of 0.069 mm when the potential evaporation increased by 1 mm in this study area. In addition, it could be found that the variation trend of the runoff sensitivity coefficient to precipitation was just opposite to that of runoff to potential evaporation (Figure 6). Because the increment of precipitation increased the watershed runoff, the increase of potential evaporation changed surface water from liquid into gas and reduced watershed runoff [69].

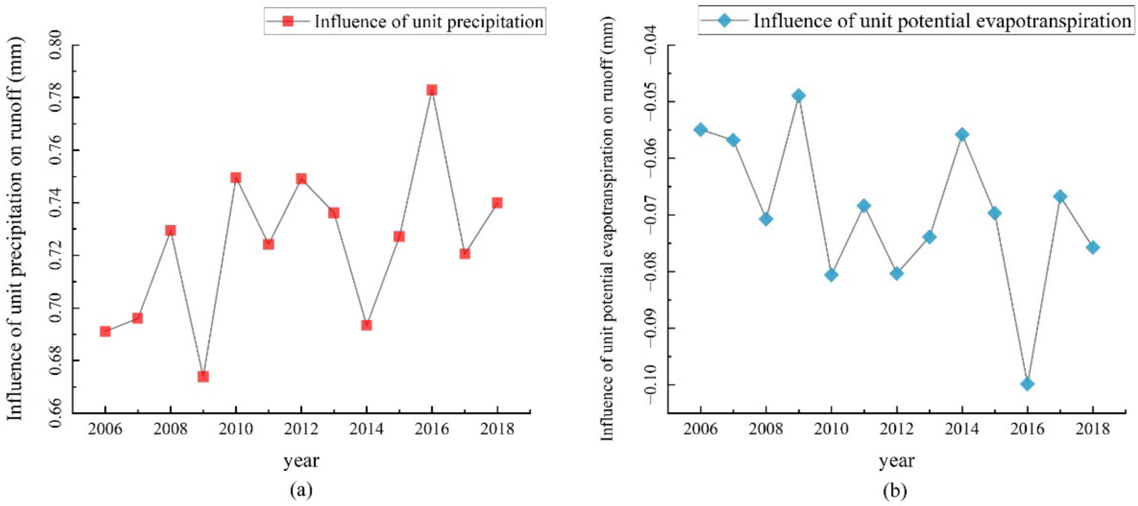

Figure 6. Impact of unit precipitation and unit potential evaporation changes on runoff depth. (**a**,**b**) were the variations of runoff depth when unit precipitation and unit potential evaporation increased, respectively.

3.6. Correlation Degrees between Socioeconomic Indicators and Runoff as Well as Runoff Depth

Previous research pointed out that socioeconomic development and human activities affected the underlying surface structure and hydrological process of the watershed to a certain extent, thus impacting the runoff [70]. High population density, rapid socioeconomic development and urbanization impacted the surface water and belowground water a lot in this region. The residential, industrial and agricultural water usage were affected as well [14]. It can be learnt that population density (POD) had the highest correlation degrees with runoff compared with other socioeconomic development indicators in 2010 and 2014 (Figure 7). Although it decreased from 0.847 in 2010 to 0.807 in 2018, it was still the second highest correlation degree, which was only second to per capita industrial output value (PIO). It indicated that the high population density and the relative human activities were an important aspect that affected watershed runoff during socioeconomic development, although the impact became weak in the later period. The higher population density increased the proportion of impervious surface, thus inhibiting the water infiltration, increasing the runoff, and increasing the urban flood risk as well [71,72]. Thus, the permeable ground could be constructed to mitigate flood risk caused by the urban surface runoff to a certain extent [73]. The correlation degree between runoff and PIO in 2010 and 2014 was second only to that of POD and it was the highest among all the socioeconomic indicators in 2018. This was because industrial activities such as industrial water use, industrial land development and industrial population gathering affected the hydrodynamic field and fluctuated the groundwater level [74].

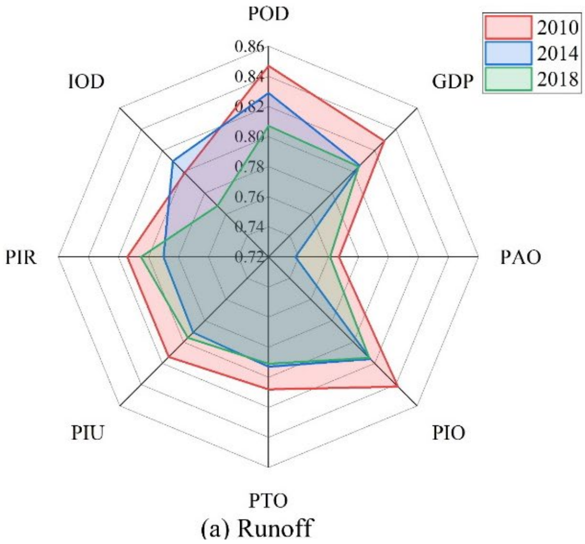

Figure 7. Correlation degrees between socioeconomic development indicators and runoff as well as runoff depth. Abbreviation: per capita gross domestic product (GDP, CNY), population density (POD, person/km^2), per capita agricultural output value (PAO, CNY), per capita industrial output value (PIO, CNY), per capita tertiary output value (PTO, CNY), per capita disposable income of urban residents (PIU, PIU), per capita disposable income of rural residents (PIR, CNY), industrial output density (IOD, CNY/m^2).

The runoff depth had the highest correlation degrees and second highest correlation degrees with per capita disposable income of rural residents (PIR) and per capita disposable income of urban residents (PIU) in 2010, 2014 and 2018, respectively. This reflected the significant impacts of the economic development in rural and urban areas on runoff depth compared with other socioeconomic development indicators. In addition, the correlation degrees between per capita gross domestic product (GDP) and runoff were the third highest in 2010 and 2018, respectively, and its correlation degrees with runoff depth ranked fourth among the eight socioeconomic development indicators in 2010, 2014 and 2018. Per capita tertiary output value (PTO) ranked the third in terms of correlation degrees with runoff depth in 2010 and 2014. It indicated that the economic development and the development of the tertiary industry in this region had become important factors affecting its water resources [75,76]. Industrial output density (IOD) had low correlation degrees with runoff and runoff depth in all selected years, which reflected its weak correlation degrees with local water resource.

4. Conclusions

The study analyzed the spatial and temporal changes of runoff as well as runoff depth in the north of Beijing-Tianjin-Hebei region and their responses to driving factors such as land use change, landscape pattern evolution, climate change and socioeconomic development during 2006–2018. The results of the space-time analysis showed that the runoff and runoff depth increased at the later stage of the study period. Runoff had an imbalanced distribution and there was rich water resource in central and south central areas.

The forest in the north basin and the grassland in the central and north region had a negative effect on runoff because the permeability and the water conductivity of the forest soil were high. This negative effect also occurred in the bare land in the southeast region.

While artificial surface and land use intensity had positive impacts on runoff and runoff depth in most areas of the basin. Moreover, the complex landscape diverted the runoff, which caused a significant negative correlation between the runoff and the mean shape index during the whole study period. A landscape with a high Shannon's diversity index enhanced the blocking effect on runoff and reduced the runoff depth.

Increased rainfall and decreased temperature as well as potential evaporation promoted the runoff and the runoff depth in many periods. In addition, the runoff depth would increase by 0.724 mm when the precipitation increased by 1mm and decrease by 0.069 mm when the potential evaporation increased by 1 mm according to the Budyko theory. The population density had the highest correlation with the runoff among all the socioeconomic development indicators in 2010 and 2014, and runoff depth had the highest and the second highest correlation degrees with PIR and PIU. This reflected the significant pressure of population and economic development on local water resource. This study would provide scientific evidence for basin water resources protection under multiple factors naturally and socially.

Supplementary Materials: The following supporting information can be downloaded at: https://www.mdpi.com/article/10.3390/rs15041027/s1, Figure S1: Geographically and temporally weighted regression between land use and runoff in 2006; Figure S2: Geographically and temporally weighted regression between land use and runoff in 2010; Figure S3: Geographically and temporally weighted regression between land use and runoff in 2014; Figure S4: Geographically and temporally weighted regression between land use and runoff depth in 2006; Figure S5: Geographically and temporally weighted regression between land use and runoff depth in 2010; Figure S6: Geographically and temporally weighted regression between land use and runoff depth in 2014; Figure S7: Geographically and temporally weighted regression between land use and runoff depth in 2018; Figure S8: Correlations between runoff and runoff depth as well as landscape indexes in 2006, 2010, 2014 and 2018; Table S1: Accuracy of geographically and temporally weighted regression.

Author Contributions: Z.F.: Methodology, Modelling, Software, Writing—Original draft. S.L.: Data curation, Modelling, Software, Visualization. Y.G.: Resources, Methodology, Formal analysis. X.L.: Conceptualization, Investigation, Funding acquisition, Review. All authors have read and agreed to the published version of the manuscript.

Funding: This research was funded by the Qinghai Province Key Research and Development and Transformation Program, grant number [2023-QY-205] and Jiangxi Province Key Research and Development Project, grant number [20212BBG73017].

Data Availability Statement: Data is available upon reasonable request.

Conflicts of Interest: The authors declare no conflict of interest.

References

1. Sample, D.J.; Liu, J. Optimizing rainwater harvesting systems for the dual purposes of water supply and runoff capture. *J. Clean. Prod.* **2014**, *75*, 174–194. [CrossRef]
2. Butt, M.J.; Bilal, M. Application of snowmelt runoff model for water resource management. *Hydrol. Process.* **2011**, *25*, 3735–3747. [CrossRef]
3. Lu, C.; Song, Z.; Wang, W.; Zhang, Y.; Si, H.; Liu, B.; Shu, L. Spatiotemporal variation and long-range correlation of groundwater depth in the Northeast China Plain and North China Plain from 2000~2019. *J. Hydrol. Reg. Stud.* **2021**, *37*, 100888. [CrossRef]
4. Rahmati, O.; Golkarian, A.; Biggs, T.; Keesstra, S.; Mohammadi, F.; Daliakopoulos, I.N. Land subsidence hazard modeling: Machine learning to identify predictors and the role of human activities. *J. Environ. Manag.* **2019**, *236*, 466–480. [CrossRef]
5. Zhang, Z.; Luo, G.; Wang, Z.; Liu, C.; Li, Y.; Jiang, X. Study on sustainable utilization of groundwater in North China Plain. *Resour. Sci.* **2009**, *31*, 355–360.
6. Oliveira, K.D.; Tomasella, J.; Del'Arco Sanches, L. Spatial-temporal analysis of the climatic and anthropogenic influences on runoff in the Jucu River Basin, Southeastern Brazil. *Land Degrad. Dev.* **2019**, *30*, 2073–2087. [CrossRef]
7. Sajikumar, N.; Remya, R.S. Impact of land cover and land use change on runoff characteristics. *J. Environ. Manag.* **2015**, *161*, 460–468. [CrossRef]
8. Moniruzzaman, M.; Thakur, P.K.; Kumar, P.; Ashraful Alam, M.; Garg, V.; Rousta, I.; Olafsson, H. Decadal Urban Land Use/Land Cover Changes and Its Impact on Surface Runoff Potential for the Dhaka City and Surroundings Using Remote Sensing. *Remote Sens.* **2020**, *13*, 83. [CrossRef]

9. Hosseiny, H.; Crimmins, M.; Smith, V.B.; Kremer, P. A Generalized Automated Framework for Urban Runoff Modeling and Its Application at a Citywide Landscape. *Water* **2020**, *12*, 357. [CrossRef]
10. Boardman, J.; Evans, R. The measurement, estimation and monitoring of soil erosion by runoff at the field scale: Challenges and possibilities with particular reference to Britain. *Prog. Phys. Geogr. Earth Environ.* **2020**, *44*, 31–49. [CrossRef]
11. Love, D.; Uhlenbrook, S.; Corzo-Perez, G.; Twomlow, S.; van der Zaag, P. Rainfall–interception–evaporation–runoff relationships in a semi-arid catchment, northern Limpopo basin, Zimbabwe. *Hydrol. Sci. J.* **2010**, *55*, 687–703. [CrossRef]
12. Rasmussen, R.; Liu, C.; Ikeda, K.; Gochis, D.; Yates, D.; Chen, F.; Tewari, M.; Barlage, M.; Dudhia, J.; Yu, W.; et al. High-Resolution Coupled Climate Runoff Simulations of Seasonal Snowfall over Colorado: A Process Study of Current and Warmer Climate. *J. Clim.* **2011**, *24*, 3015–3048. [CrossRef]
13. Yuan, Z.; Pang, Y.; Gao, J.; Liu, X.; Sheng, H.; Zhuang, Y. Improving quantification of rainfall runoff pollutant loads with consideration of path curb and field ridge. *Resour. Environ. Sustain.* **2021**, *6*, 100042. [CrossRef]
14. Zhou, C.; Gong, H.; Chen, B.; Gao, M.; Cao, Q.; Cao, J.; Duan, L.; Zuo, J.; Shi, M. Land Subsidence Response to Different Land Use Types and Water Resource Utilization in Beijing-Tianjin-Hebei, China. *Remote Sens.* **2020**, *12*, 457. [CrossRef]
15. Hunt, A. Soil formation, vegetation growth, and water balance: A theory for Budyko. *Hydrogeol. Chem. Weather. Soil Form.* **2021**, *1*, 67–80. [CrossRef]
16. Pirnia, A.; Golshan, M.; Darabi, H.; Adamowski, J.; Rozbeh, S. Using the Mann–Kendall test and double mass curve method to explore stream flow changes in response to climate and human activities. *J. Water Clim. Chang.* **2019**, *10*, 725–742. [CrossRef]
17. Fotheringham, A.S.; Crespo, R.; Yao, J. Geographical and Temporal Weighted Regression (GTWR). *Geogr. Anal.* **2015**, *47*, 431–452. [CrossRef]
18. Huang, B.; Wu, B.; Barry, M. Geographically and temporally weighted regression for modeling spatio-temporal variation in house prices. *Int. J. Geogr. Inf. Sci.* **2010**, *24*, 383–401. [CrossRef]
19. Zhang, J.; Zhang, A.; Li, J.; Li, F.; Peng, J. Gray Correlation Analysis and Prediction on Permanent Deformation of Subgrade Filled with Construction and Demolition Materials. *Materials* **2019**, *12*, 3035. [CrossRef]
20. Feng, Z.; Wang, L.; Peng, Q.; Li, J.; Liang, T. Effect of environmental factors on soil properties under different land use types in a typical basin of the North China Plain. *J. Clean. Prod.* **2022**, *344*, 131084. [CrossRef]
21. Wei, X.; Sun, H.; Chen, Z.; Li, X.; Wei, H.; Jia, W.; Li, W. Element migration and enrichment characteristics of bedrock–regolith–soil–plant continuum system in the chestnut planting area, Chengde, China. *Acta Geochim.* **2022**, *41*, 839–860. [CrossRef]
22. Wei, M.; Huang, S.; Li, L.; Zhang, T.; Akram, W.; Khatoon, Z.; Renaud, F.G. Evolution of water quality and biota in the Panjiakou Reservoir, China as a consequence of social and economic development: Implications for synergies and trade-offs between Sustainable Development Goals. *Sustain. Sci.* **2021**, *17*, 1385–1404. [CrossRef]
23. Yang, Y.; Zhao, T.; Wang, Y.; Shi, Z. Research on impacts of population-related factors on carbon emissions in Beijing from 1984 to 2012. *Environ. Impact Assess. Rev.* **2015**, *55*, 45–53. [CrossRef]
24. Dai, D.; Sun, M.; Lv, X.; Lei, K. Evaluating water resource sustainability from the perspective of water resource carrying capacity, a case study of the Yongding River watershed in Beijing-Tianjin-Hebei region, China. *Environ. Sci. Pollut. Res.* **2020**, *27*, 21590–21603. [CrossRef]
25. Guan, D.; Hubacek, K.; Tillotson, M.; Zhao, H.; Liu, W.; Liu, Z.; Liang, S. Lifting China's water spell. *Environ. Sci. Technol.* **2014**, *48*, 11048–11056. [CrossRef]
26. Peng, S.; Ding, Y.; Liu, W.; Li, Z. 1 km monthly temperature and precipitation dataset for China from 1901 to 2017. *Earth Syst. Sci. Data* **2019**, *11*, 1931–1946. [CrossRef]
27. Shi, C.; Yuan, S.; Shi, C.; Zhao, T. Effects of climate change and human activities on runoff in Luanhe Basin. *J. Soil Water Conserv.* **2018**, *32*, 264–269.
28. Milly, P.C.D.; Dunne, K.A. Colorado River flow dwindles as warming-driven loss of reflective snow energizes evaporation. *Science* **2020**, *367*, 1252–1255. [CrossRef]
29. Milly, P.C.; Dunne, K.A. Potential evaporation and continental drying. *Nat. Clim. Chang.* **2016**, *6*, 946–949. [CrossRef]
30. He, Q.; Huang, B. Satellite-based mapping of daily high-resolution ground PM2.5 in China via space-time regression modeling. *Remote Sens. Environ.* **2018**, *206*, 72–83. [CrossRef]
31. Lu, B.; Harris, P.; Charlton, M.; Brunsdon, C. The GWmodel R package: Further topics for exploring spatial heterogeneity using geographically weighted models. *Geo-Spat. Inf. Sci.* **2014**, *17*, 85–101. [CrossRef]
32. Yang, J.; Huang, X. The 30 m annual land cover dataset and its dynamics in China from 1990 to 2019. *Earth Syst. Sci. Data* **2021**, *13*, 3907–3925. [CrossRef]
33. Azzeh, M.; Neagu, D.; Cowling, P.I. Fuzzy grey relational analysis for software effort estimation. *Empir. Softw. Eng.* **2010**, *15*, 60–90. [CrossRef]
34. Zheng, C.; Li, R.; Hu, M.; Zou, L. Determination of low-temperature crack control parameter of binding asphalt materials based on gray correlation analysis. *Constr. Build. Mater.* **2019**, *217*, 226–233. [CrossRef]
35. Chengde Statistical Bureau. *Chengde Statistical Yearbook*; China Statistics Press: Beijing, China, 2006–2018.
36. Šímová, P.; Gdulová, K. Landscape indices behavior: A review of scale effects. *Appl. Geogr.* **2012**, *34*, 385–394.
37. Kuchma, T.; Tarariko, O.; Syrotenko, O. Landscape Diversity Indexes Application for Agricultural Land Use Optimization. *Procedia Technol.* **2013**, *8*, 566–569. [CrossRef]

38. Rets, E.P.; Durmanov, I.N.; Kireeva, M.B. Peak Runoff in the North Caucasus: Recent Trends in Magnitude, Variation and Timing. *Water Resour.* **2019**, *46*, S56–S66. [CrossRef]
39. Yang, Y.; Tian, F. Abrupt change of runoff and its major driving factors in Haihe River Catchment, China. *J. Hydrol.* **2009**, *374*, 373–383. [CrossRef]
40. Lorente, C.; Causapé, J.; Glud, R.N.; Hancke, K.; Merchán, D.; Muñiz, S.; Val, J.; Navarro, E. Impacts of agricultural irrigation on nearby freshwater ecosystems: The seasonal influence of triazine herbicides in benthic algal communities. *Sci. Total Environ.* **2015**, *503-504*, 151–158. [CrossRef]
41. Men, B.; Liu, H.; Tian, W.; Wu, Z.; Hui, J. The Impact of Reservoirs on Runoff Under Climate Change: A Case of Nierji Reservoir in China. *Water* **2019**, *11*, 1005. [CrossRef]
42. Nyssen, J.; Clymans, W.; Descheemaeker, K.; Poesen, J.; Vandecasteele, I.; Vanmaercke, M.; Zenebe, A.; Van Camp, M.; Haile, M.; Haregeweyn, N.; et al. Impact of soil and water conservation measures on catchment hydrological response—A case in north Ethiopia. *Hydrol. Process.* **2010**, *24*, 1880–1895. [CrossRef]
43. Appels, W.M.; Bogaart, P.W.; van der Zee, S.E. Surface runoff in flat terrain: How field topography and runoff generating processes control hydrological connectivity. *J. Hydrol.* **2016**, *534*, 493–504. [CrossRef]
44. Mahmoud, S.H. Investigation of rainfall–runoff modeling for Egypt by using remote sensing and GIS integration. *Catena* **2014**, *120*, 111–121. [CrossRef]
45. Muñoz-Villers, L.E.; McDonnell, J.J. Land use change effects on runoff generation in a humid tropical montane cloud forest region. *Hydrol. Earth Syst. Sci.* **2013**, *17*, 3543–3560. [CrossRef]
46. Miller, J.D.; Kim, H.; Kjeldsen, T.R.; Packman, J.; Grebby, S.; Dearden, R. Assessing the impact of urbanization on storm runoff in a peri-urban catchment using historical change in impervious cover. *J. Hydrol.* **2014**, *515*, 59–70. [CrossRef]
47. Alaoui, A.; Caduff, U.; Gerke, H.H.; Weingartner, R. Preferential Flow Effects on Infiltration and Runoff in Grassland and Forest Soils. *Vadose Zone J.* **2011**, *10*, 367–377. [CrossRef]
48. Dunnett, N.; Nagase, A.; Booth, R.; Grime, P. Influence of vegetation composition on runoff in two simulated green roof experiments. *Urban Ecosyst.* **2008**, *11*, 385–398. [CrossRef]
49. Silva, L.L. Are basin and reservoir tillage effective techniques to reduce runoff under sprinkler irrigation in Mediterranean conditions? *Agric. Water Manag.* **2017**, *191*, 50–56. [CrossRef]
50. Hümann, M.; Schüler, G.; Müller, C.; Schneider, R.; Johst, M.; Caspari, T. Identification of runoff processes—The impact of different forest types and soil properties on runoff formation and floods. *J. Hydrol.* **2011**, *409*, 637–649. [CrossRef]
51. Brauman, K.A.; Freyberg, D.L.; Daily, G.C. Forest structure influences on rainfall partitioning and cloud interception: A comparison of native forest sites in Kona, Hawai'i. *Agric. For. Meteorol.* **2010**, *150*, 265–275. [CrossRef]
52. Tian, T.; Mou, F.; Wang, J.; Zhao, L.; Chen, L.; Li, Q. Impact of land use change on surface runoff in the main urban area of Chongqing. *Res. Soil Water Conserv.* **2021**, *28*, 128–135.
53. Singh, R.J.; Deshwal, J.; Sharma, N.; Ghosh, B.; Bhattacharyya, R. Effects of conservation tillage based agro-geo-textiles on resource conservation in sloping croplands of Indian Himalayan Region. *Soil Tillage Res.* **2019**, *191*, 37–47. [CrossRef]
54. Ly, A.; Marsman, M.; Wagenmakers, E.J. Analytic posteriors for Pearson's correlation coefficient. *Stat. Neerl.* **2018**, *72*, 4–13. [CrossRef] [PubMed]
55. Zhang, S.; Fan, W.; Li, Y.; Yi, Y. The influence of changes in land use and landscape patterns on soil erosion in a watershed. *Sci. Total Environ.* **2017**, *574*, 34–45. [CrossRef]
56. Wang, Z.; Wang, F.; Wu, B. Changes of the wetland landscape and the consequent impacts on the waterbirds in Western Songnen plain. *Procedia Environ. Sci.* **2011**, *10*, 2608–2613.
57. Zhang, Y.; Bi, Z.; Zhang, X.; Yu, Y. Influence of Landscape Pattern Changes on Runoff and Sediment in the Dali River Watershed on the Loess Plateau of China. *Land* **2019**, *8*, 180. [CrossRef]
58. Zhang, N.; Luo, Y.-J.; Chen, X.-Y.; Li, Q.; Jing, Y.-C.; Wang, X.; Feng, C.-H. Understanding the effects of composition and configuration of land covers on surface runoff in a highly urbanized area. *Ecol. Eng.* **2018**, *125*, 11–25. [CrossRef]
59. Ma, Y.; Zhao, H. The Role of Spatial Patterns of Low Impact Development in Urban Runoff Pollution Control within Parcel Based Catchments. *Front. Environ. Sci.* **2022**, *10*, 989. [CrossRef]
60. Yan, Y.; Zhao, C.; Wang, C.; Shan, P.; Zhang, Y.; Wu, G. Ecosystem health assessment of the Liao River Basin upstream region based on ecosystem services. *Acta Ecol. Sin.* **2016**, *36*, 294–300. [CrossRef]
61. Chiew, F.H.S.; Potter, N.J.; Vaze, J.; Petheram, C.; Zhang, L.; Teng, J.; Post, D.A. Observed hydrologic non-stationarity in far south-eastern Australia: Implications for modelling and prediction. *Stoch. Environ. Res. Risk Assess.* **2014**, *28*, 3–15. [CrossRef]
62. Miao, C.; Ashouri, H.; Hsu, K.-L.; Sorooshian, S.; Duan, Q. Evaluation of the PERSIANN-CDR Daily Rainfall Estimates in Capturing the Behavior of Extreme Precipitation Events over China. *J. Hydrometeorol.* **2015**, *16*, 1387–1396. [CrossRef]
63. Potter, N.J.; Chiew, F.H.S. An investigation into changes in climate characteristics causing the recent very low runoff in the southern Murray-Darling Basin using rainfall-runoff models. *Water Resour. Res.* **2011**, *47*, W00G10. [CrossRef]
64. Roderick, M.L.; Farquhar, G.D. A simple framework for relating variations in runoff to variations in climatic conditions and catchment properties. *Water Resour. Res.* **2011**, *47*. [CrossRef]
65. Peel, M.C.; McMahon, T.A.; Finlayson, B.L. Vegetation impact on mean annual evaporation at a global catchment scale. *Water Resour. Res.* **2010**, *46*, W09508. [CrossRef]

66. Berghuijs, W.R.; Larsen, J.R.; Van Emmerik, T.H.M.; Woods, R.A. A Global Assessment of Runoff Sensitivity to Changes in Precipitation, Potential Evaporation, and Other Factors. *Water Resour. Res.* **2017**, *53*, 8475–8486. [CrossRef]
67. Trancoso, R.; Larsen, J.R.; McAlpine, C.; McVicar, T.R.; Phinn, S. Linking the Budyko framework and the Dunne diagram. *J. Hydrol.* **2016**, *535*, 581–597. [CrossRef]
68. Donohue, R.J.; Roderick, M.L.; McVicar, T.R. Assessing the differences in sensitivities of runoff to changes in climatic conditions across a large basin. *J. Hydrol.* **2011**, *406*, 234–244. [CrossRef]
69. Liu, Q.; McVicar, T.R. Assessing climate change induced modification of Penman potential evaporation and runoff sensitivity in a large water-limited basin. *J. Hydrol.* **2012**, *464*, 352–362. [CrossRef]
70. Guan, X.; Zhang, J.; Bao, Z.; Liu, C.; Jin, J.; Wang, G. Past variations and future projection of runoff in typical basins in 10 water zones, China. *Sci. Total Environ.* **2021**, *798*, 149277. [CrossRef]
71. Kim, H.W.; Kim, J.-H.; Li, W.; Yang, P.; Cao, Y. Exploring the impact of green space health on runoff reduction using NDVI. *Urban For. Urban Green.* **2017**, *28*, 81–87. [CrossRef]
72. Schoener, G. Urban Runoff in the U.S. Southwest: Importance of Impervious Surfaces for Small-Storm Hydrology. *J. Hydrol. Eng.* **2018**, *23*, 05017033. [CrossRef]
73. Miller, J.D.; Hess, T. Urbanisation impacts on storm runoff along a rural-urban gradient. *J. Hydrol.* **2017**, *552*, 474–489. [CrossRef]
74. Chen, S.; Liu, F.; Zhang, Z.; Zhang, Q.; Wang, W. Changes of groundwater flow field of Luanhe River Delta under the human activities and its impact on the ecological environment in the past 30 years. *China Geol.* **2021**, *4*, 455–462. [CrossRef]
75. Bhave, A.G.; Conway, D.; Dessai, S.; Stainforth, D.A. Water Resource Planning Under Future Climate and Socioeconomic Uncertainty in the Cauvery River Basin in Karnataka, India. *Water Resour. Res.* **2018**, *54*, 708–728. [CrossRef]
76. Willuweit, L.; O'Sullivan, J.J.; Shahumyan, H. Simulating the effects of climate change, economic and urban planning scenarios on urban runoff patterns of a metropolitan region. *Urban Water J.* **2016**, *13*, 803–818. [CrossRef]